Interface-Induced Room-Temperature Ferromagnetism in Hydrogenated Epitaxial Graphene

A. J. M. Giesbers,[1,*] K. Uhlířová,[2] M. Konečný,[1,4] E. C. Peters,[3] M. Burghard,[3] J. Aarts,[2] and C. F. J. Flipse[1,†]

[1]*Molecular Materials and Nanosystems, Eindhoven University of Technology, 5600 MB Eindhoven, Netherlands*
[2]*Magnetic and Superconducting Materials, Leiden Institute of Physics, 2333 CA Leiden, Netherlands*
[3]*Max-Planck Institute for Solid State Research, Heisenbergstrasse 1, D-70569 Stuttgart Germany*
[4]*CEITEC BUT, Technická 10, 616 69 Brno, Czech Republic*

(Received 27 May 2013; revised manuscript received 10 September 2013; published 16 October 2013)

We show ferromagnetic properties of hydrogen-functionalized epitaxial graphene on SiC. Ferromagnetism in such a material is not directly evident as it is inherently composed of only nonmagnetic constituents. Our results nevertheless show strong ferromagnetism with a saturation of $0.9\mu_B$/hexagon projected area, which cannot be explained by simple magnetic impurities. The ferromagnetism is unique to hydrogenated epitaxial graphene on SiC, where interactions with the interfacial buffer layer play a crucial role. We argue that the origin of the observed ferromagnetism is governed by electron correlation effects of the narrow Si dangling bond states in the buffer layer exchange coupled to localized states in the hydrogenated graphene layer. This forms a quasi-three-dimensional ferromagnet with a Curie temperature higher than 300 K.

DOI: 10.1103/PhysRevLett.111.166101 PACS numbers: 68.65.Pq, 75.50.Pp, 75.70.−i

Graphene represents a close-to-ideal material for spintronic applications [1] due to its capability of ballistic transport over micrometer distances [2], as well as its very long spin relaxation time and spin relaxation length [3,4]. In this context, considerable effort has recently been directed to rendering graphene ferromagnetic via chemical modification. Thus far, ferromagnetic order in graphene has been attained through covalent functionalization, involving the linkage of radical species like the spin-bearing carbon atom of an organic molecule or hydrogen atoms to the graphene layer [5–17]. Along these lines, functionalization of epitaxial graphene by aryl radicals has been reported to yield disordered magnetism, comprising a mixture of ferromagnetic, superparamagnetic, and antiferromagnetic regions [18]. With the aid of combined atomic and magnetic force microscopy, it could be proven that these randomly dispersed regions are constituted by the attached moieties. This lack of a periodic functionalization pattern of the graphene sheet prevents the achievement of long range ferromagnetic order, thus limiting the use of such samples in spintronic devices. Furthermore, room temperature ferromagnetism has been detected in partially hydrogenated epitaxial graphene grown on silicon carbide (SiC) and attributed to hydrogen monomers bonded to the graphene sheet [12]. Despite these accomplishments, however, both the mechanism underlying the ferromagnetic ordering, and the role played by the SiC substrate used for the epitaxial graphene growth, has not yet been clarified. Here, we experimentally demonstrate that ferromagnetism in hydrogenated epitaxial graphene originates from the interaction between localized states in the hydrogenated graphene and silicon dangling bonds in the underlying buffer layer. In addition, we show that the created magnetic areas are distributed over the entire graphene-buffer layer surface, thus enabling to effectively tune the overall magnetization through the density of attached hydrogen atoms.

To explore the ferromagnetism in epitaxial graphene, we use samples grown on insulating 6H-SiC substrates following the procedure described in Ref. [19] (all samples originate from the same wafer). The atomic force micrograph (AFM) of the sample surface [Fig. 1(a)] reveals terrace steps originating from a slight miscut of the SiC substrate. The terraces are typically 3–5 um wide and approximately 10 nm high and are overgrown with a continuous carpet of graphene [20,21]. The inset in Fig. 1(a) shows a schematic cross section of the layer sequence at the surface with a graphene layer on top of an interfacial carbon layer (buffer layer) partly bonded to the SiC substrate. On the terrace edges, an unintentional region of bilayer graphene has formed under the current growth conditions [19], discernible as brighter areas in the corresponding atomic force micrograph phase image [Fig. 1(b)]. The presence of a small bilayer area is confirmed by Raman microscopy and low energy electron microscopy investigations (see Supplemental Material Fig. S1 [22]) and has the same coverage in all samples. After growth, the graphene samples are hydrogenated by an atomic hydrogen source in an ultrahigh vacuum chamber for different exposure times. Successful hydrogenation is testified by an enhancement of the sp^3 defect associated Raman D peak, whose intensity increases with treatment time [Figs. 1(c) and 1(d)], as discussed in more detail in the Supplemental Material [22]. Increasing hydrogen exposure also leads to a rising C-H signal in x-ray photoabsorption spectra (see Supplemental Material [22]). The inset in Fig. 1(d) illustrates the hydrogen bonded on the top graphene layer.

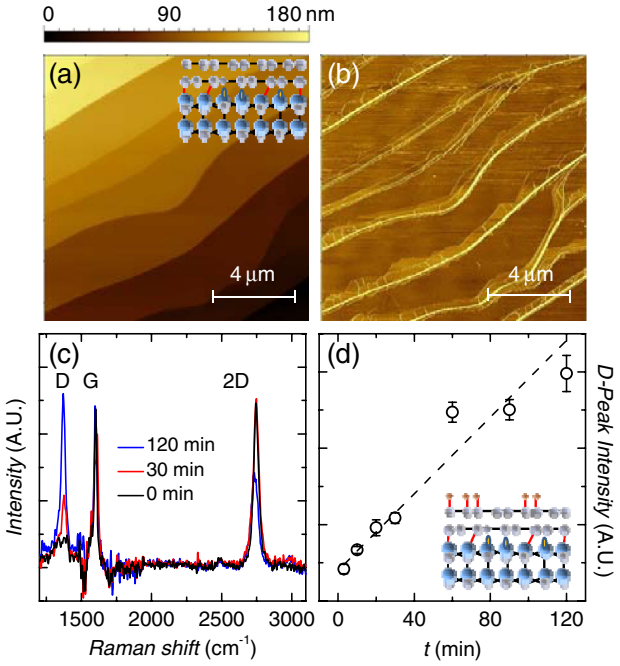

FIG. 1 (color online). (a) Atomic force micrograph of the typical SiC terrace structure on top of which the graphene is grown. The inset shows a schematic of the surface structure with from top to bottom a graphene layer, a buffer layer, and the SiC substrate. The gray spheres represent carbon, the blue spheres silicon, and the yellow ovals the silicon dangling bonds. (b) Phase image showing the single layer graphene areas on top of the terraces and the narrow bilayer regions at the terrace edges. (c) Raman spectra of hydrogenated graphene with a treatment time $t = 0$ min. (black), 30 min. (red), and 120 min. (blue). Clearly visible is the upcoming D-peak intensity with increasing treatment time. (d) D-peak intensity as a function of treatment time (the line is a guide to the eye). The inset shows the schematic bonding of hydrogen (orange spheres) to the graphene layer.

The magnetic properties of the hydrogenated graphene samples are determined using a commercial superconducting quantum interference device (SQUID) with a sensitivity of 5×10^{-8} emu. All measurements are performed at room temperature unless stated otherwise. Figure 2(a) shows the magnetization of an epitaxial graphene sample hydrogenated for three minutes. The linear background is related to the bulk SiC diamagnetism and can be subtracted by a linear fit to the high field part of the curve where all other forms of magnetism are assumed to be saturated. The resulting diamagnetic susceptibility $\chi = \mu_0 M/Hm$, with $m = (1.97 \pm 0.05) \times 10^{-5}$ kg the sample mass and $\mu_0 = 4\pi \times 10^{-7}$ Tm/A the vacuum permeability, is $\chi_{\mathrm{SiC}} = -(4.1 \pm 0.1) \times 10^{-9}$ m^3/kg, within its error in good agreement with literature ($\chi_{\mathrm{SiC}} = -4.01 \times 10^{-9}$ m^3/kg). Consistent values for χ_{SiC}, within the error range, were found for all samples used in this Letter. The data obtained after subtraction of the SiC diamagnetic background are shown in Fig. 2(b) for three different temperatures. The curves show a clear ferromagnetic response from the hydrogenated epitaxial graphene. The hysteresis loop shows a saturation magnetization of $M_s = \pm 27 \times 10^{-7}$ emu, a remanent magnetization of $M_r = \pm 7 \times 10^{-7}$ emu, and a coercive field of $H_c = \pm 91$ Oe at 300 K. Upon decreasing the temperature, a small increase in the high field magnetization occurs. A similar trend is observed for the coercive field and the remanent magnetization [inset Fig. 2(b)]. The measured saturation magnetization at room temperature corresponds to a value of about $0.9\mu_B$ per hexagon projected area. We use the term "projected area" to include magnetic interface contributions, which will be discussed later.

Figure 2(c) compares the ferromagnetic signal for the 3 min hydrogenated sample under in-plane magnetic field, along ($\theta = 0°$), and perpendicular ($\theta = 90°$) to the terraces as well as for out-of-plane (OofP) orientation [inset Fig. 2(c)]. A notable anisotropy can be discerned, with easier magnetization along the terrace steps (black curve), as compared to perpendicular alignment (red curve) and the out-of-plane direction (blue curve). This difference manifests itself in a lower saturation magnetization and in the case of the out-of-plane signal in a more stretched hysteresis loop. The preferred magnetization along the terrace edges might result from the predominant formation of double site hydrogen sites aligned along the zigzag direction of graphene [23]. The double H sites show elongated shaped charge structures of 3 nm or more with sixfold symmetry coinciding with the sixfold symmetry of the graphene honeycomb lattice. In atomic resolution scanning tunneling microscopy, it was shown that the armchair edge of the graphene layer coincides with the SiC terrace structure [24]. Combined, these results lead to anisotropy between the terrace edge and perpendicular to the edge direction which could explain the observed anisotropy in the magnetization. The out-of-plane magnetization contribution is probably due to a noncollinear spin orientation in the buffer layer, similar as for the $\sqrt{3} \times \sqrt{3}R30$ $6H$-SiC(0001) structure of SiC [25].

To tune the ferromagnetic signal, we can use the hydrogen coverage, as is shown in Fig. 2(d) for hydrogenation times between 0 and 120 minutes. While the pristine graphene (0 min, black curve) displays no magnetic signal, a short hydrogen exposure (0.5 min, red curve) results in a clear ferromagnetic signal. From the corresponding hysteresis loop, a coercive field of $H_c = \pm 65$ Oe and remanent magnetization of $M_r = \pm 2.4 \times 10^{-7}$ emu is extracted. At high fields (H = 3000 Oe), the magnetization reaches a saturation value of 14×10^{-7} emu. This saturation magnetization, M_s, increases up to a treatment time of 3 min (27×10^{-7} emu), which is followed by a decrease for longer treatments, finally resulting in M_s (120 min) = 13×10^{-7} emu. The same trend is observed in the coercive field and the remanent magnetization for the different samples.

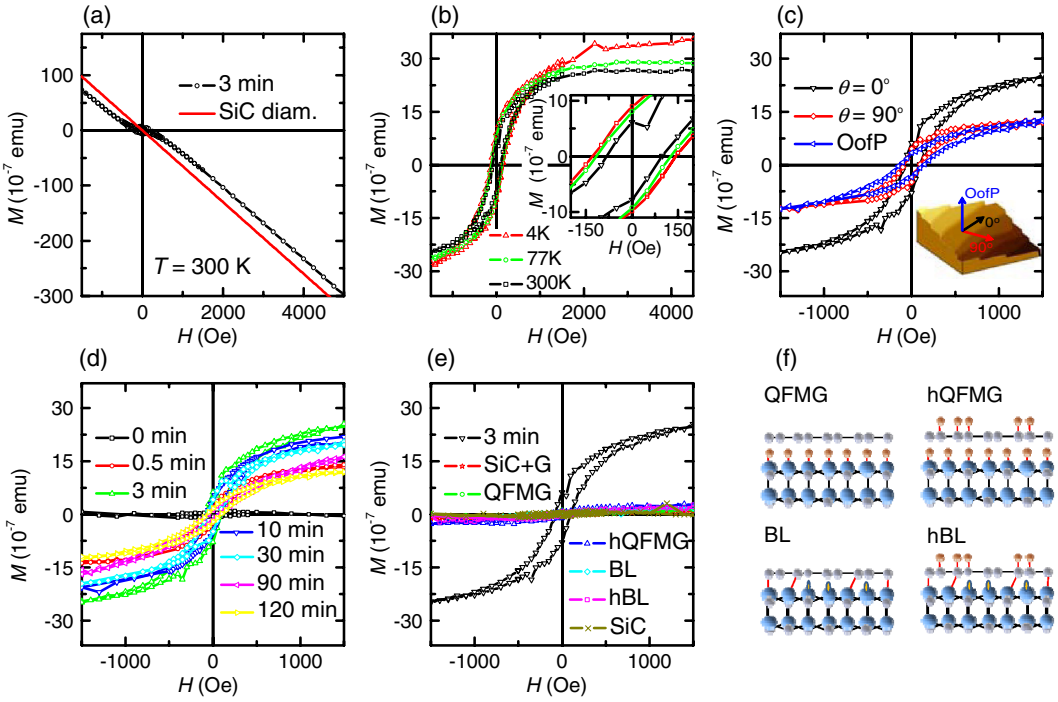

FIG. 2 (color online). (a) Room temperature magnetization of hydrogenated epitaxial graphene as a function of the applied magnetic field for hydrogenated epitaxial graphene treated for three minutes. The red line shows the diamagnetic contribution of the SiC substrate. (b) Temperature dependence of the magnetization after subtraction of the diamagnetic background showing a clear ferromagnetic hysteresis loop. The inset shows a zoom of the coercive field and remanent magnetization (3 min treatment). (c) Direction dependence of the magnetization (3 min treatment). (d) Ferromagnetic signal for different hydrogen treatment times, $t = 0$, 0.5, 3, 10, 30, 90, and 120 minutes. (e) Magnetization for different control samples. (f) Schematic representations of the various control samples.

In order to determine the origin of the ferromagnetic behavior, we have investigated the magnetization properties of several control samples [Fig. 2(e)]. Firstly, a sample prepared in the same manner as the 3 minute sample, except that the hydrogen bottle is kept closed, is found to exhibit no ferromagnetic signal (red curve). Secondly, the same procedure is applied to an untreated bare SiC sample, which likewise does not lead to ferromagnetic signatures (dark yellow curve). Thirdly, to test the influence of the underlying substrate, a quasi-freestanding monolayer of graphene [25] (QFMG) is used as a control sample [Fig. 2(f) shows a schematic]. It is obtained by growing only a buffer layer [25–27] on the SiC, followed by hydrogen intercalation to passivate the SiC substrate and turn the buffer layer into a QFMG. Owing to the reduced substrate interaction, QFMG is of superior quality compared to epitaxial graphene [25]. Pristine QFMG samples not subjected to hydrogenation (exemplified by green curve) do not display ferromagnetism as expected for pure graphene (in total two samples were studied). Remarkably, also after three minutes of hydrogenation, no ferromagnetic signal at room temperature emerges for such samples [hQFMG, schematic in Fig. 2(f)] (blue curve representative for one out of two samples). The above findings highlight that the hydrogenated graphene is not ferromagnetic at room temperature and the buffer layer is crucial to render the epitaxial graphene ferromagnetic. Finally, in a fourth control experiment using two buffer layer samples (one shown, cyan curve) and three hydrogenated buffer layer samples (one shown, magenta curve) no ferromagnetic signal is detected [schematics of the samples are shown in Fig. 2(f)]. This absence consolidates that hydrogenated epitaxial graphene requires both the hydrogenated graphene and the underlying buffer layer to become ferromagnetic. At low temperatures, the linear background magnetization, observable for both the buffer layer samples and the hQFMG, leads to a smaller χ_{SiC} compared to the pure SiC substrates. This difference hints toward an unsaturated low temperature paramagnetic contribution in these samples, akin to fluorinated graphene laminates [28]. The presence of localized paramagnetic-like states in the buffer layer was recently also suggested from spin transport experiments in epitaxial graphene [29]. In our preliminary high magnetic field magnetization measurements, the paramagnetism of the buffer layer is indeed confirmed, saturating at $H/T \approx 25$ kOe/K (see Supplemental Material Fig. S4 [22]). The crucial role of the buffer layer also indicates that the measured saturation magnetization in the hydrogenated epitaxial graphene samples of $0.9\mu_B$ per hexagon projected area is not solely

from the graphene layer but is distributed between the two layers.

Further insight into the ferromagnetic properties of the hydrogenated graphene is gained by detecting the remanent magnetization with the aid of magnetic force microscopy (MFM) (see Fig. 3). By placing the sample briefly on either the south pole ($-B$) or north pole ($+B$) of a permanent magnet prior to MFM measurements, we can magnetize the sample in, respectively, a negative or positive out-of-plane remanent magnetization state as we observed in the SQUID measurements of Fig. 2(c). Figures 3(a) and 3(b) show the magnetic signal of the same area for the two magnetization directions with their respective cross sections in panel 3(c). The highlighted dirt particle is an artifact due to cross talk with the topography [30] and serves as a position marker on the sample. The topology of the sample is similar to Figs. 1(a) and 1(b). The clear difference in MFM contrast between the single (1L) and bilayer (2L) areas, indicate their different magnetization. This might be due to different hydrogen coverages [31,32], in accord with the lower overall D-peak intensity on the bilayer regions observed in Raman images. Other possible contributions are the different electronic structure of the bilayer graphene, as well as different interactions among the hydrogen sites, or in the specific case of the bilayer graphene between hydrogen sites and the buffer layer due to the increased distance between the buffer layer and the hydrogenated layer. In the SQUID measurements, the bilayer areas will reduce the overall saturation magnetization, however since the bilayer coverage is similar for all samples, the results above are not affected. The switching of the out-of-plane remanent magnetization direction is clearly visible in the MFM cross sections in Fig. 3(c).

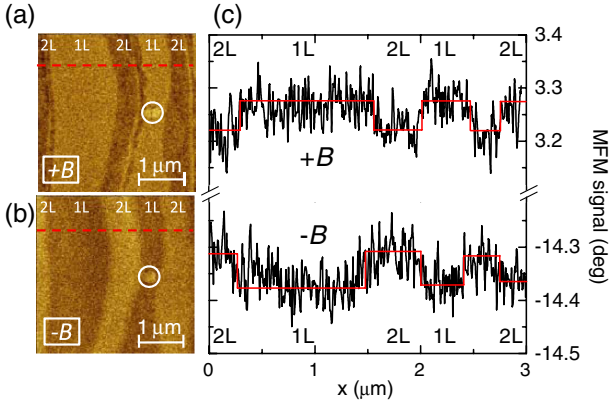

FIG. 3 (color online). (a) Magnetic force micrograph of hydrogenated epitaxial graphene after applying a positive magnetic field to the sample showing high and low remanent magnetization for single and bilayer, respectively (scale: $+3.3° \pm 0.2°$). (b) Inversion of the remanent magnetization after applying a negative magnetic field to the sample (scale: $-14.4° \pm 0.2°$). (c) Cross section of the positive (a) and negative (b) magnetization. We repeated the switching between positive and negative magnetization several times yielding the same result.

Specifically, after positive B-field magnetization, the MFM signal is positive and the signal from the single layer is slightly larger than that from the bilayer. After negative B-field magnetization, the MFM signal has reversed the sign and the response from the single layer is again highest. These changes show that the color inversion between panel 3(a) and 3(b) is due to a complete flip of the magnetization direction, while the signal from the single layer is always higher (either more positive or more negative) than that from the bilayer. That the flip is not symmetric around zero indicates a constant background phase shift and might be attributed to electrostatic interactions simultaneously probed by the metallic tip. Electric field microscopy confirmed this magnetic-field independent electrostatic background [33] (see Supplemental Material Fig. S3 [22]).

The MFM measurements corroborate the ferromagnetism of the hydrogenated epitaxial graphene sample and show that the signal originates from the whole surface. Together with the observed variation of the ferromagnetic strength with hydrogen coverage, the magnetic anisotropy, and control sample magnetic measurements, these results form a conclusive set of observations which rule out any possible magnetic contaminations as the origin of the observed magnetic behavior.

The observed ferromagnetism in our hydrogenated epitaxial graphene is best interpreted in terms of an exchange coupled interaction between localized electron states of the buffer layer and localized states formed by sp^3 defects of the hydrogenated graphene layer [23]. The overall paramagnetic behavior of the buffer layer indicates the presence of localized magnetic moments, which are the localized defect states, attributed to Si dangling bonds (DB), forming an insulating behavior as has been shown by scanning tunneling microscopy and spectroscopy experiments [34,35]. Upon hydrogen adsorption on top of the graphene layer, carbon-hydrogen bonds are created, forming sp^3 defect states [23]. These localized midgap states can be spin split in filled and unfilled localized states close to the Fermi level due to the Coulomb interaction of the Si DB states of the buffer layer, forming a quasi-three-dimensional ferromagnetic state with a Curie temperature (T_C) of 300 K or higher. However, hydrogenated graphene can also be intrinsically ferromagnetic (or superparamagnetic) [36] with a much lower Curie temperature due to its two dimensionality, which would become quasi-three-dimensional if the paramagnetic buffer layer will exchange couple to it, and thereby, raise T_C. Alternatively, the midgap states do not necessarily have to be spin split but could mediate a coupling between the spin polarized buffer layer states and thereby, introduce a ferromagnetic system.

To conclude, hydrogenated epitaxial graphene shows a ferromagnetic behavior with a Curie temperature higher than 300 K and a magnetic moment of $0.9\mu_B$ per carbon hexagon projected area. We have shown that both the hydrogen coverage and the buffer layer with the Si

dangling bonds play a crucial role for the high temperature ferromagnetic properties. To explain the ferromagnetism in our graphene system at room temperature, we tentatively propose an exchange coupled interaction between the Coulomb induced localized Si DB states of the buffer layer and the localized midgap state or the two-dimensional ferromagnetic hydrogenated graphene layer. The buffer layer stabilizes the ferromagnetic behavior at room temperature and this quasi-three-dimensional system can explain the relatively high Curie temperature, higher than 300 K. The high Curie temperature in combination with a small coercive field (100 Oe) and high spin relaxation time in graphene makes hydrogenated epitaxial graphene a favorable material for spintronic applications.

This work has been supported by the Dutch Organization for Scientific Research (NWO) under Project No. NWO-nano 11447, and by the European Regional Development Fund under Project No. CEITEC-CZ.1.05/1.1.00/02.0068. We thank M. W. G. M. Verhoeven for help with the XPS experiments, D. B. Boltje for the LEEM experiments, and M. Herps for high-field SQUID experiments.

*A.J.M.Giesbers@tue.nl
†C.F.J.Flipse@tue.nl

[1] A. Candini, S. Klyatskaya, M. Ruben, W. Wernsdorfer, and M. Affronte, Nano Lett. **11**, 2634 (2011).
[2] D.-K. Ki, D. Jeong, J.-H. Choi, H.-J. Lee, and K.-S. Park, Phys. Rev. B **78**, 125409 (2008).
[3] N. Tombros, C. Jozsa, M. Popinciuc, H. T. Jonkman, and B. J. van Wees, Nature (London) **448**, 571 (2007).
[4] T. Maassen, J. J. van den Berg, N. IJbema, F. Fromm, Th. Seyller, R. Yakimova, and B. J. van Wees, Nano Lett. **12**, 1498 (2012).
[5] L. Chen, D. Yu, and F. Liu, Appl. Phys. Lett. **93**, 223106 (2008).
[6] Y.-W. Son, M. L. Cohen, and S. G. Louie, Nature (London) **444**, 347 (2006).
[7] J. Hong, E. Bekyarova, P. Liang, W. A. de Heer, R. C. Haddon, and S. Khizroev, Sci. Rep. **2**, 624 (2012).
[8] L. Brey, H. A. Fertig, and S. Das Sarma, Phys. Rev. Lett. **99**, 116802 (2007).
[9] P. O. Lehtinen, A. S. Foster, A. Ayuela, A. Krasheninnikov, K. Nordlund, and R. M. Nieminen, Phys. Rev. Lett. **91**, 017202 (2003).
[10] M. Wu, E.-Z. Liu, and J. Z. Jiang, Appl. Phys. Lett. **93**, 082504 (2008).
[11] D. W. Boukhvalov, M. I. Katsnelson, and A. I. Lichtenstein, Phys. Rev. B **77**, 035427 (2008).
[12] L. Xie, X. Wang, J. Lu, Z. Ni, Z. Luo, H. Mao, R. Wang, Y. Wang, H. Huang, D. Qi, R. Liu, T. Yu, Z. Shen, T. Wu, H. Peng, B. Özyilmaz, K. Loh, A. T. S. Wee, Ariando, and W. Chen, Appl. Phys. Lett. **98**, 193113 (2011).
[13] D. W. Boukhvalov and M. I. Katsnelson, J. Phys. Condens. Matter **21**, 344205 (2009).
[14] T. Kuila, S. Bosea, A. K. Mishrab, P. Khanraa, N. H. Kimc, and J. H. Leea, Prog. Mater. Sci. **57**, 1061 (2012).
[15] W. Wei and X. Qu, Small **8**, 2138 (2012).
[16] M. Papagno, S. Rusponi, P. M. Sheverdyaeva, S. Vlaic, M. Etzkorn, D. Pacilé, P. Moras, C. Carbone, and H. Brune, ACS Nano **6**, 199 (2012).
[17] J. W. Suk, R. D. Piner, J. An, and R. S. Ruoff, ACS Nano **4**, 6557 (2010).
[18] J. Hong, S. Niyogi, E. Bekyarova1, M. Itkis1, P. Ramesh, N. Amos, D. Litvinov, C. Berger, W. A. de Heer, S. Khizroev, and R. C. Haddon, Small **7**, 1175 (2011).
[19] K. V. Emtsev, A. Bostwick, K. Horn, J. Jobst, G. L. Kellogg, L. Ley, J. L. McChesney, T. Ohta, S. A. Reshanov, J. Röhrl, E. Rotenberg, A. K. Schmid, D. Waldmann, H. B. Weber, and Th. Seyller, Nat. Mater. **8**, 203 (2009).
[20] W. Norimatsu and M. Kusunoki, Physica (Amsterdam) E **42**, 691 (2010).
[21] S. W. Poon, W. Chen, A. T. S. Wee, and E. S. Tok, Phys. Chem. Chem. Phys. **12**, 13 522 (2010).
[22] See Supplemental Material at http://link.aps.org/supplemental/10.1103/PhysRevLett.111.166101 for details on sample preparation and additional sample characterization by Raman, LEEM, XPS, EFM and SQUID.
[23] M. Scheffler *et al.*, ACS Nano **6**, 10 590 (2012).
[24] T. W. Hu, D. Y. Ma, F. Ma, and K. W. Xu, Appl. Phys. Lett. **101**, 241903 (2012).
[25] F. Speck, J. Jobst, F. Fromm, M. Ostler, D. Waldmann, M. Hundhausen, H. B. Weber, Th. Seyller, Appl. Phys. Lett. **99**, 122106 (2011).
[26] N. Ferralis, R. Maboudian, and C. Carraro, Phys. Rev. Lett. **101**, 156801 (2008).
[27] K. V. Emtsev, F. Speck, Th. Seyller, L. Ley, and J. D. Riley, Phys. Rev. B **77**, 155303 (2008).
[28] R. R. Nair, M. Sepioni, I.-L. Tsai, O. Lehtinen, J. Keinonen, A. V. Krasheninnikov, T. Thomson, A. K. Geim, and I. V. Grigorieva, Nat. Phys. **8**, 199 (2012).
[29] T. Maassen, J. J. van den Berg, E. H. Huisman, H. Dijkstra, F. Fromm, Th. Seyller, and B. J. van Wees, Phys. Rev. Lett. **110**, 067209 (2013).
[30] P. J. A. Schendel, H. J. van Hug, B. Stiefel, S. Martin, and H.-J. Güntherodt, J. Appl. Phys. **88**, 435 (2000).
[31] Z. Luo, T. Yu, K.-J. Kim, Z. Ni, Y. You, S. Lim, Z. Shen, S. Wang, and J. Lin, ACS Nano **3**, 1781 (2009).
[32] S. Ryu, M. Y. Han, J. Maultzsch, T. F. Heinz, P. Kim, M. L. Steigerwald, and L. E. Brus, Nano Lett. **8**, 4597 (2008).
[33] D. Martínez-Martín, M. Jaafar, R. Pérez, J. Gómez-Herrero, and A. Asenjo, Phys. Rev. Lett. **105**, 257203 (2010).
[34] A. Nie and R. M. Feenstra, J. Vac. Sci. Technol. A **27**, 1052 (2009).
[35] J. Cervenka, K. van der Ruit, and C. F. J. Flipse, Phys. Status Solidi A **207**, 595 (2010); Phys. Rev. B **81**, 205403 (2010).
[36] O. V. Yazyev, Rep. Prog. Phys. **73**, 056501 (2010).